Publications of the Astronomical Society of Australia (2023), **40**, e058, 11 pages
doi:10.1017/pasa.2023.55

CAMBRIDGE UNIVERSITY PRESS

Research Article

Inviscid protostellar disc ring formation and high-density ring edges due to the ejection and subsequent infall of material onto a protostellar disc

Kurt Liffman

Centre for Astrophysics and Super Computing, Swinburne University of Technology, Hawthorn, VIC 3122, Australia

Abstract

Discs of gas and dust are ubiquitous around protostars. Hypothetical viscous interactions within the disc are thought to cause the gas and dust to accrete onto the star. Turbulence within the disc is theorised to be the source of this disc viscosity. However, observed protostellar disc turbulence often appears to be small and not always conducive to disc accretion. In addition, theories for disc and planet evolution have difficulty in explaining the observed disc rings/gaps which form much earlier than expected.

Protostellar accretion discs are observed to contain significant quantities of dust and pebbles. Observations also show that some of this material is ejected from near the protostar, where it travels to the outer regions of the disc. Such solid infalling material has a relatively small amount of angular momentum compared to the material in the disc. This infalling material lowers the angular momentum of the disc and should drive a radial flow towards the protostar.

We show that the local radial accretion speed of the disc is proportional to the mass rate of infalling material onto the disc. Higher rates of infall onto the disc implies higher radial accretion disc speeds. As such, regions with high rates of infall of gas, dust, and pebbles onto the disc will produce gaps on relatively short timescales in the disc, while regions associated with relative low rates of infalling material will produce disc rings. As such, the inner edge of a disc gap will tend to have a higher surface density, which may enhance the probability of planet formation. In addition, the outer edge of a disc gap will act as a dust trap and may also become a site for planet formation.

For the early Solar System, such a process may have collected O^{16}-poor forsterite dust from the inner regions of the protosolar disc and O^{16}-rich CAIs and AOAs from the inner edge regions of the protosolar disc, thereby constructing a region favourable to the formation of pre-chondritic planetesimals.

Keywords: protoplanetary discs; stars; protostars

(Received 19 May 2023; revised 25 October 2023; accepted 30 October 2023)

1. Introduction

When first formed, protostellar systems consist of a central protostar surrounded by a disc of gas and dust, where the disc accretes material onto the star (Williams & Cieza, 2011). The source of the energy loss that allows material to flow from the disc to the star has long been a source of theoretical speculation (Martin et al., 2019). Most models use magnetic or hydrodynamic instabilities (Balbus & Hawley, 1991; Fromang & Lesur, 2019) to create turbulence which, in turn, produces viscous effects within the disc (Frank et al., 2002). The standard α disc model being based on various assumptions regarding disc turbulence (Shakura & Sunyaev, 1973).

These are useful models that are probably applicable to protostellar discs in certain regions and at particular stages of formation, but, to date, there is little observational evidence to support the presence of wide scale, significant turbulence in many protostellar discs (Flaherty et al., 2017; Teague et al., 2018).

Corresponding author: K. Liffman; Email: kliffman@swin.edu.au.

Cite this article: Liffman K. (2023) Inviscid protostellar disc ring formation and high-density ring edges due to the ejection and subsequent infall of material onto a protostellar disc. *Publications of the Astronomical Society of Australia* **40**, e058, 1–11. https://doi.org/10.1017/pasa.2023.55

In the absence of wide scale disc turbulence, disc magnetic fields have long been suggested as a plausible driver of disc accretion, (Bai, 2016; Weiss et al., 2021). Unfortunately, it is not easy to detect magnetic fields in protostellar systems, however, meteorites may provide additional information regarding magnetic fields in the solar protostellar system (Borlina et al., 2021).

Observations suggest that sub-mm and mm to cm-sized particles are abundant in protostellar discs (Ohashi & Kataoka, 2019; Macías et al., 2021). These observations are also consistent with the observed high abundance of such particles (e.g., chondrules, Calcium Aluminium Inclusions (CAIs), Amoeboid Olivine Aggregates (AOAs) &c) found in primitive meteorites (Bizzarro et al., 2017).

Standard disc theory, would suggest that all these particles should quickly drift into the protostar (Weidenschilling, 1977). It is possible that turbulence within discs can transport particulate material from the inner to the outer regions of the disc (Zhou et al., 2022). However, the observed low disc turbulence and prominent gaps in even the youngest protostellar discs (van der Marel et al., 2019) suggests that this upstream turbulent advection of particulate material within protostellar discs may be of limited effect.

© The Author(s), 2023. Published by Cambridge University Press on behalf of the Astronomical Society of Australia. This is an Open Access article, distributed under the terms of the Creative Commons Attribution-NonCommercial-NoDerivatives licence (http://creativecommons.org/licenses/by-nc-nd/4.0/), which permits non-commercial re-use, distribution, and reproduction in any medium, provided that no alterations are made and the original article is properly cited. The written permission of Cambridge University Press must be obtained prior to any commercial use and/or adaptation of the article.

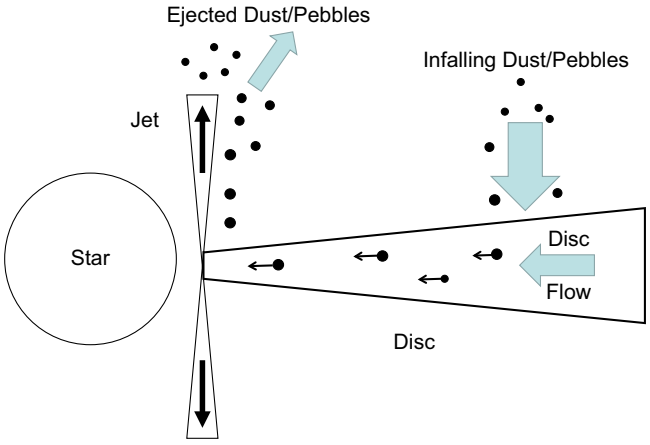

Figure 1. Low angular momentum particles are ejected from the inner disc and land in the outer regions of the disc, where they are returned to the inner disc by radial inflow and/or radial drift, thereby renewing the cycle. The removal of angular momentum from the outer disc produces disc flow towards the star. For the disc as a whole, this is likely to be a small effect and more conventional sources of disc accretion are probably required to drive accretion onto the protostar.

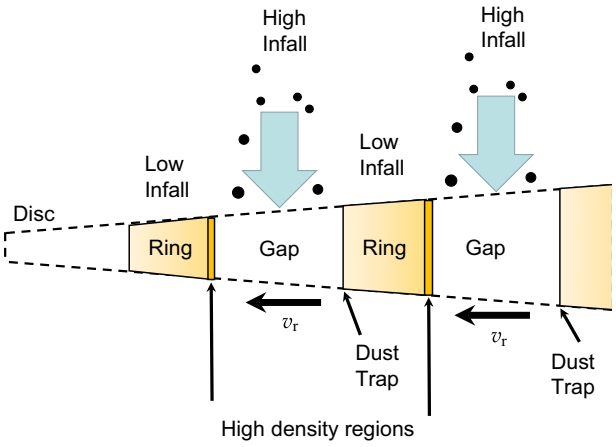

Figure 2. Sections of the disc that suffer high rates of infalling material will have a higher radial disc speed, v_r, which will help produce disc gaps on a relatively short timescale. Conversely, low infall rates will produce low radial disc speeds and rings of disc material. The material in the gap regions will flow into the ring regions. The outer regions of the rings will, therefore, have enhanced densities and pressures, while the inner regions of the rings will act as dust traps, so both ring edges may provide fertile ground for planet formation.

In addition, Spitzer Space Telescope and James Webb Space Telescope observations also demonstrate that crystalline, micron-sized particles are ejected from the inner regions of protostars and travel radially across the face of the disc and re-enter the disc some au from the protostar or are completely ejected from the protostellar system (Poteet et al., 2011; Juhász et al., 2012; Ábrahám et al., 2019; Kóspál et al., 2023). These particles from the inner regions of the disc will tend to have little or no angular momentum relative to material in the outer regions of the disc. When these ejected particles re-enter the disc at greater distances, then the angular momentum of the outer disc is reduced, and the outer disc regions will move radially inwards towards the protostar.

It is plausible that the entrained dust and small pebbles can move with the gas or drift back to the inner disc region where the outflow is located. These particles may then be re-ejected to the outer regions of the disc and a repeating, virtuous cycle is produced that drives disc accretion into the inner regions of the accretion disc, whereupon conventional sources of viscosity can drive accretion onto the protostar (Figure 1).

This cycle can potentially replenish the pebbles in the disc (Hansen, 2014) and thereby counter the expected relatively fast drift of pebbles into the protostar (Weidenschilling, 1977; Brauer et al., 2007, 2008). However, the deduced mass accretion rates from this effect will likely be small relative to what is observed. This occurs because the mass of dust/pebbles in the disc will be of order 1% of the disc mass. This implies that the solid material has to be cycled around approximately 100 times to have a major influence in driving material onto the protostar.

However, this infalling material is observed, at least in one case, to be heterogeneously distributed across the accretion disc (Juhász et al., 2012; Ábrahám et al., 2019; Kóspál et al., 2023). Some theoretical models (e.g., Giacalone et al. (2019)) also explicitly predict that disc winds will deposit particulate material outside the outflow region. So, there may be discrete regions of the disc that are strongly affected by infalling material.

The theory presented here shows that the radial speed of disc material is proportional to the local mass rate of infall. If there are spatial or temporal inhomogeneities in this infalling material, then there will also be variations in the local radial speed of the disc moving towards the protostar. Higher mass infall regions will have a higher local radial disc speed, while lower mass infall regions will have a relatively lower radial disc speed. Such inhomogeneities will produce gaps and rings in the disc on a relatively short timescale. Higher mass infall will produce gaps, while lower mass infall will produce rings. Due to this accretion behaviour, the material in the gaps will flow into the outer edges of the rings and these regions will have enhanced densities and pressures, which may aid in planet formation (Figure 2). In addition, the outer edges of the gaps will tend to have a pressure profile which will trap dust (Pinilla et al., 2012). So, planetesimal formation may become more likely at both the inner and outer edges of the gaps.

In this initial model, we do not consider the back reaction of the inward drifting pebbles on the disc gas (e.g., Nakagawa et al. (1986)). This back reaction on the gas would tend to cause the entire gas disc to increase in size and help conserve angular momentum for the entire disc. As such, we do not consider the angular momentum behaviour of a whole disc, but only consider the affect of angular momentum loss in discrete sections of a disc.

We also do not consider infall of material from a molecular cloud core onto a nascent protostellar disc. From Kuznetsova et al. (2022), it is clear that such infalling material can intercept the disc in regions with significantly different angular momentum. Kuznetsova et al. (2022) use a full hydrodynamic code (albeit with approximations in the boundary conditions and code to make the problem computationally tractable) to illustrate how discrete, low angular momentum infalling material from a molecular cloud core can produce gaps and rings in a protostellar disc. The simplified disc evolution equations derived in this paper are also applicable as they apply to any case where material rains down upon a disc.

This paper is organised as follows: in Section 2 we derive the infall disc equations; in Section 3 these equations are solved analytically to illustrate ring and gap formation on relatively short timescales in a protostellar disc; in Section 4 we discuss the 'chicken and egg' problem of ring/gap versus planet formation, where we suggest that formation of rings and gaps is the necessary foundation for planet formation.

https://doi.org/10.1017/pasa.2023.55 Published online by Cambridge University Press

2. Disc equations with infall

As discussed in Falcke & Melia (1997) and Appendix A, the equation for mass conservation in a disc with infalling material is

$$r\frac{\partial \Sigma}{\partial t} = -\frac{\partial (r v_{\rm r} \Sigma)}{\partial r} + r\dot{\Sigma}_{\rm i}, \tag{1}$$

with r the radial cylindrical coordinate, t the time, $\Sigma(r,t)$ the surface density of the disc, $v_{\rm r}$ the radial velocity of the flow of disc material and $\dot{\Sigma}_{\rm i}(r,t)$ the total rate of infall of material per unit area and time onto the disc, where we note that, in this paper, the infall is assumed to be symmetric on *both* sides of the disc.

The infalling material may arise from the ambient medium around the protostellar system. The derived equations do not discriminate between gaseous and particulate material. However, in this paper, we assume that it arises due to the action of the protostellar jet flow and/or disc winds that eject solid material to different heights above the disc and different distances from the protostar. As such, the particulate material will return to the disc on a range of timescales. It is also possible that solid material will be ejected from the disc via disc winds and/or a semiquiescent jet flow. Whatever the exact ejection mechanism, we note that observations require particulate material to be ejected from the inner disc to the outer regions of the disc.

The angular momentum equation is tentatively:

$$r\frac{\partial \left(\Sigma r^2 \Omega\right)}{\partial t} = -\frac{\partial \left(v_{\rm r} \Sigma r^3 \Omega\right)}{\partial r} + \frac{1}{2\pi}\frac{\partial Q}{\partial r} + \dot{\Sigma}_{\rm i} r^3 \Omega_{\rm i}, \tag{2}$$

where $\Omega(r,t)$ and $\Omega_{\rm i}(r,t)$ are the angular speeds of the disc and infalling material, respectively. $Q(r,t) = 2\pi\nu\Sigma r^3 \frac{\partial \Omega}{\partial r}$ is the disc viscous torque, with ν the disc viscosity.

We suppose that the standard astrophysical disc viscosity is only significant and applicable at the initial stage(s) of disc formation or in the very inner regions of the disc. it is certainly possible that early forming planets or companion stars can also induce disc accretion onto the protostar, but we shall ignore such possibilities. Given these constraints, disc turbulence is taken to be negligible and $\nu \approx 0$, which implies that $Q \approx 0$ for most protostellar discs. The disc angular momentum equation becomes:

$$r\frac{\partial \left(\Sigma r^2 \Omega\right)}{\partial t} = -\frac{\partial \left(v_{\rm r} \Sigma r^3 \Omega\right)}{\partial r} + \dot{\Sigma}_{\rm i} r^3 \Omega_{\rm i}, \tag{3}$$

As derived in Appendix B, the disc radial speed, $v_{\rm r}$, from equations (1) and (3), is

$$v_{\rm r} = \frac{1}{\frac{\partial (r^2\Omega)}{\partial r}}\frac{\dot{\Sigma}_{\rm i}}{\Sigma} r^2 (\Omega_{\rm i} - \Omega). \tag{4}$$

For Keplerian angular disc speed, (i.e., $\Omega \approx \sqrt{GM_*/r^3}$, where G is the gravitational constant and M_* the mass of the central object) we have:

$$\begin{aligned} v_{\rm r} &= 2r\frac{\dot{\Sigma}_{\rm i}}{\Sigma}\left(\frac{\Omega_{\rm i}}{\Omega} - 1\right) \\ &\approx 0.95 \text{ mm s}^{-1} \left(\frac{r}{1\text{au}}\right)\left(\frac{\dot{\Sigma}_{\rm i}/\Sigma}{10^{-7}/\text{yr}}\right)\left(\frac{\Omega_{\rm i}}{\Omega} - 1\right). \end{aligned} \tag{5}$$

If the angular speed of the infalling material is greater than the angular speed of the disc material then we would expect outward movement of the disc material, where the reverse is true if the angular speed of the infalling material is less than the angular speed of the disc.

The mass flow rate or accretion rate, $\dot{M}_a$, within the disc has the form:

$$\begin{aligned} \dot{M}_a &= 2\pi r \Sigma v_{\rm r} = \frac{2\pi}{\frac{\partial (r^2\Omega)}{\partial r}} \dot{\Sigma}_{\rm i} r^3 (\Omega_{\rm i} - \Omega) \\ &= 4\pi r^2 \dot{\Sigma}_{\rm i}\left(\frac{\Omega_{\rm i}}{\Omega} - 1\right) \\ &\approx 3.4 \times 10^{-10} \text{M}_\odot/\text{yr} \left(\frac{r}{1\text{au}}\right)^2 \left(\frac{\dot{\Sigma}_{\rm i}}{10^{-7}\Sigma/\text{yr}}\right)\left(\frac{\Omega_{\rm i}}{\Omega} - 1\right). \end{aligned} \tag{6}$$

The characteristic flow rate of mass onto the protostar is small relative to what is observed. However, the mass flow rate is directly proportional to surface density rate of infalling material: $\dot{\Sigma}_{\rm i}$. If the infalling material is distributed inhomogeneously across the disc and $\dot{\Sigma}_{\rm i}$ has a local value that is relatively high, then $\dot{M}_a$ is large and a local disc gap may form. Conversely, if $\dot{\Sigma}_{\rm i}$ has a local value that is small, then $\dot{M}_a$ is relatively small and a disc ring may arise at that radial distance in the disc.

As the infalling material impacts the disc, it loses kinetic energy, which can be dissipated as radiation at the disc surface. So the total rate of energy dissipated per unit area, $D_{\rm i}$ by both sides of the disc, will be:

$$\begin{aligned} D_{\rm i} &\approx \frac{1}{2}\dot{\Sigma}_{\rm i}\left(u_{\phi{\rm i}} - u_\phi\right)^2 + \frac{1}{2}\dot{\Sigma}_{\rm i} u_{\rm ri}^2 \\ &= \frac{1}{2}\dot{\Sigma}_{\rm i} r^2\Omega^2\left(\frac{\Omega_{\rm i}}{\Omega} - 1\right)^2 + \frac{1}{2}\dot{\Sigma}_{\rm i} u_{\rm ri}^2, \end{aligned} \tag{7}$$

with $u_{\phi{\rm i}} = r\Omega_{\rm i}$, $u_\phi = r\Omega$, and $u_{\rm ri}(r)$ is the radial speed of the infalling material as it impacts the disc at a distance r from the protostar. A lower bound on the energy dissipated can be obtained if we set $u_{\rm ri} \approx 0$ and assume Keplerian disc rotation,

$$\begin{aligned} D_{\rm i} &\approx \frac{1}{2}\dot{\Sigma}_{\rm i} r^2\Omega^2\left(\frac{\Omega_{\rm i}}{\Omega} - 1\right)^2 = \frac{GM_*\dot{M}_a}{8\pi r^3}\left(\frac{\Omega_{\rm i}}{\Omega} - 1\right) \\ &\approx 0.01 \text{ Jm}^{-2}\text{s}^{-1}\left(\frac{(M_*/\text{M}_\odot)(\dot{M}_a/10^{-10}\text{ M}_\odot/\text{yr})}{(r/\text{au})^3}\right) \\ &\times \left(\frac{\Omega_{\rm i}}{\Omega} - 1\right), \end{aligned} \tag{8}$$

The energy dissipation given in equation (8) is approximately one third of the energy dissipation for a standard viscous accretion disc (Frank et al., 2002). The energy dissipated by one side of the disc will be half the above number.

Finally, the time evolution of the disc surface density is obtained by combining equations (1) and (5):

$$\begin{aligned} \frac{\partial \Sigma}{\partial t} &= -2r\frac{\partial \dot{\Sigma}_{\rm i}}{\partial r}\left(\frac{\Omega_{\rm i}}{\Omega} - 1\right) - 4\dot{\Sigma}_{\rm i}\left(\frac{\Omega_{\rm i}}{\Omega} - 1\right) \\ &- 2r\dot{\Sigma}_{\rm i}\left(\frac{1}{\Omega}\frac{\partial \Omega_{\rm i}}{\partial r} - \frac{\Omega_{\rm i}}{\Omega^2}\frac{\partial \Omega}{\partial r}\right) + \dot{\Sigma}_{\rm i}. \end{aligned} \tag{9}$$

In this paper, we set the angular speed of the disc gas to be approximately Keplerian:

$$\Omega(r) \approx \sqrt{\frac{GM_*}{r^3}}. \tag{10}$$

As derived in Appendix C2 of Liffman et al. (2020), the angular speed of the infalling material that has been initially ejected from

https://doi.org/10.1017/pasa.2023.55 Published online by Cambridge University Press

the inner regions, assuming Keplerian motion, of a protostellar disc is

$$\Omega_{\rm i}(r) \approx \frac{\ell}{r^2}, \tag{11}$$

where ℓ is the specific angular momentum of the particle. For the case where a particle is launched from the distance, $r_{\rm i}$, then

$$\ell \approx \sqrt{GM_* r_{\rm i}}. \tag{12}$$

If the particles are launched from a jet flow, then $r_{\rm i}$ is assumed to be located in the innermost regions of the disc. Kóspál et al. (2023) have determined that 0.3 to 0.7 au is a realistic value for $r_{\rm i}$ - at least for the formation and initial ejection distance for micron-sized forsterite grains from the protostar Ex Lup. However, in this paper, we decided to adopt $r_{\rm i} = 0.05$ au, to act as an extreme endpoint.

It is also possible that the angular speed of the particle may be super-Keplerian due to the 'Propeller' effect of the stellar magnetosphere extending further than the co-rotation radius. In this case, the angular speed of the magnetosphere is greater than the angular speed of the disc gas. Such a situation may produce an outflow where the gas flow has super-Keplerian angular speed (Li & Wickramasinghe, 1997).

If the infalling material arises from outside the protostellar system (i.e., the protostar and protostellar disc), then $\Omega_{\rm i}$ will be set by additional factors external to the protostellar system.

3. Disc ring and gap formation

Gaps and rings in protostellar discs are quite common. To quote, van der Marel et al. (2019): 'ringlike structures are found across the full ranges of spectral type, luminosity, and age, ranging from 0.4 Myr up to 10 Myr'.

There have been many interesting proposals for how such gaps and rings could form. The formation of planets is the most common and reasonable explanation for these phenomena (ibid.). However, the observation that rings and gaps appear in discs that are less than 0.5 Myr old (Segura-Cox et al., 2020) is a challenge for planet formation theories and suggest an additional process may be required to produce gaps and rings plus enhance the probability of planet formation.

In this section, we show that gaps and rings can form relatively quickly due to the infall of low angular momentum material onto the disc. Gap formation due to infall produces over-dense regions in the outer perimeters of the resulting rings. The inner perimeters of the resulting rings may also function as dust traps. The resulting over-dense regions may provide fertile conditions for planet formation.

To illustrate ring and gap formation in a protostellar disc, we consider the case where the angular momentum of the infalling material is close to zero ($\Omega_{\rm i} \approx 0$ or $r_i \ll r$), and the rate of infall, $\dot{\Sigma}_{\rm i}$, is approximately constant in time and space over a finite region of the disc. This situation may arise, for example, when an outflow is ejecting material which subsequently returns to discrete outer regions of the disc over a limited period of time. Alternatively, we may have the infall of low angular material from any external source where the infalling material lands on a specific section of the protostellar disc (e.g., Kuznetsova et al. (2022)).

As such, equation (5) becomes

$$v_{\rm r} = \frac{dr}{dt} = -2r\frac{\dot{\Sigma}_{\rm i}}{\Sigma}, \tag{13}$$

while equation (9) has the form:

$$\frac{\partial \Sigma}{\partial t} = 5\dot{\Sigma}_{\rm i}. \tag{14}$$

These equations were first solved, semi-analytically, in Wijnen et al. (2017), who analysed the behaviour of accretion discs undergoing time-variable, face-on, infall accretion.

As discussed in Appendix C, the analytic solutions to these equations, assuming a constant rate of infalling (zero angular momentum) material onto a section of the disc, are

$$r(t) = \frac{r(t_0)}{\left(1 + (t - t_0)/\tau_{\rm g}\right)^{2/5}}, \tag{15}$$

and

$$\Sigma(r(t), t) = \Sigma(r(t_0), t_0)\left(1 + (t - t_0)/\tau_{\rm g}\right), \tag{16}$$

where t_0 is the initial time and $\tau_{\rm g}$ is the timescale for radial movement in the disc gap due to infalling material:

$$\begin{aligned}\tau_{\rm g} &= \frac{\Sigma(r(t_0), t_0)}{5\dot{\Sigma}_{\rm i}} \\ &\approx 2 \times 10^5 {\rm yr}\, \frac{\left(\frac{\Sigma(r(t_0),t_0)}{10\ {\rm kg\ m^{-2}}}\right)}{\left(\frac{\dot{\Sigma}_{\rm i}}{10^{-5}\ {\rm kg\ m^{-2} yr^{-1}}}\right)}.\end{aligned} \tag{17}$$

The scaling in equation (17) for $\Sigma(r(t_0), t_0)$ is guided by Hayashi's disc surface density (Hayashi, 1981) for a minimum mass solar protoplanetary disc at a distance of 100 au from the protostar. The value for $\dot{\Sigma}_{\rm i}$ assumes a disc mass accretion rate onto the protostar of 5×10^{-7} $M_\odot {\rm yr}^{-1}$ of which 10 % is ejected by the outflow and 1 % of the outflowing material (i.e., 5×10^{-10} $M_\odot {\rm yr}^{-1}$) is returned to the disc between a distance of 100 au to 110 au from the protostar. It would appear that gap formation timescales in the range of 10^5 to 10^6 years are plausible.

As infall progresses, the radial distance of a particular region of the disc decreases and its mass surface density increases with time. In particular, when $(t - t_0) = \tau_{\rm g}$ then $r(\tau_{\rm g}) = r(t_0)/2^{2/5} \approx 0.758 r(t_0)$ and $\Sigma(\tau_{\rm g}) = 2\Sigma(r(t_0), t_0)$. So the radial distance shrinks by about a quarter and the surface mass density doubles.

Suppose we have material raining down on a disc section, between $r_{\rm gin}$ and $r_{\rm gout}$, where the adjacent disc regions suffer relatively little or no infalling material. This affected disc region will tend to radially migrate to an inner boundary section of the disc, B, with thickness, $\Delta_{\rm B}$ and thereby produce a gap in the disc. Over time, this disc boundary section may develop a significantly enhanced density (Figure 3).

The behaviour of equations (15) and (16) in producing the disc gap is displayed in Figure 4. In Figure 4(a), the lines follow the position in the disc that is undergoing infall of material. This part of the disc moves towards the inner radius of the disc gap over time. For example, the dashed line starts at 1.1 times the inner edge of the gap (1.1 $r_{\rm gin}$) and after approximately a time of 0.3 $\tau_{\rm g}$, this portion of the disc reaches the inner edge of the gap. For Figure 4(b), increasing time is now right to left. We can again start at a distance at 1.1 times the inner edge of the gap. At the end of the disc migration, the surface density of the disc is approaching 1.3 times the original disc surface density.

https://doi.org/10.1017/pasa.2023.55 Published online by Cambridge University Press

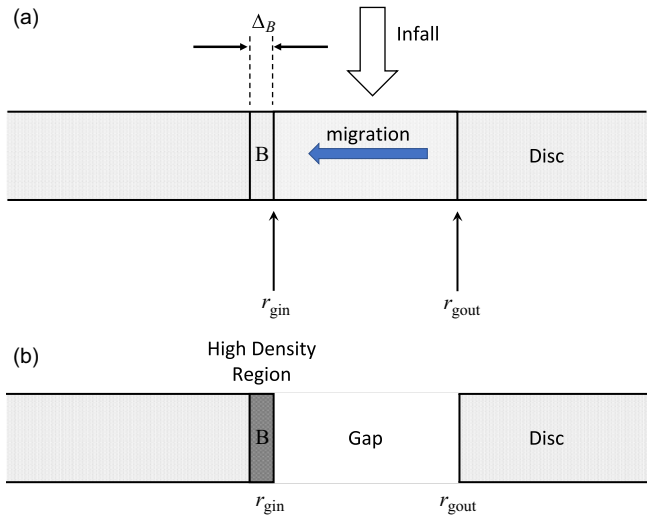

Figure 3. (a) Infalling material rains down on a section of a disc, thereby inducing radial migration of material into a boundary layer B of thickness Δ_B.(b) If the infall proceeds for a sufficiently long period of time, a gap, or a low-density region may form with a high-density region or pressure maximum region B at the inner edge of the gap.

From equation (6) the mass in the boundary section, M_B, is

$$\begin{aligned} M_B(t) &\approx -4\pi r_{gin}^2 \dot{\Sigma}_i \left(\frac{\Omega_i}{\Omega} - 1\right)(t - t_0) + M_B(t_0) \\ &\approx 4\pi r_{gin}^2 \dot{\Sigma}_i (t - t_0) + M_B(t_0) \end{aligned} \tag{18}$$

The time it takes for a particular point in the nascent disc gap to move from $r(t_0)$ to $r(t)$ can be deduced from equation (15).

$$t - t_0 = \tau_g \left(\left(\frac{r(t_0)}{r(t)} \right)^{5/2} - 1 \right). \tag{19}$$

Assuming an approximately initially similar disc surface density $\Sigma(t_0)$ in the gap region, the total time, t_G, for the gap to appear is

$$\begin{aligned} t_G - t_0 &= \tau_g \left(\left(\frac{r_{gout}}{r_{gin}} \right)^{5/2} - 1 \right) \\ &\approx \frac{\Sigma(r_{gout}, t_0)}{5\dot{\Sigma}_i} \left(\left(\frac{r_{gout}}{r_{gin}} \right)^{5/2} - 1 \right). \end{aligned} \tag{20}$$

A plot of equation (20) is given in Figure 5. As an example, to understand this graph, if the inner and outer gap radii are 100 au and 130 au, respectively, then the ratio of the two radii is 1.3. Consequently, it will approximately take a time τ_g for such a gap to form.

Substituting equation (20) into equation (18) gives the total amount of mass accreted into the boundary region, B:

$$M_B(t_G) \approx \frac{4}{5}\pi r_{gin}^2 \Sigma(r_{gout}, t_0) \left(\left(\frac{r_{gout}}{r_{gin}} \right)^{5/2} - 1 \right) + M_B(t_0) \tag{21}$$

Assuming $\Delta_B \ll r_{gin}$, the area of the boundary region is approximately $2\pi r_{gin}\Delta_B$, which, combined with equation (18), gives a boundary surface density of

$$\Sigma_B(r_{gin}, t) \approx \frac{2 r_{gin} \dot{\Sigma}_i (t - t_0)}{\Delta_B} + \Sigma_B(r_{gin}, t_0). \tag{22}$$

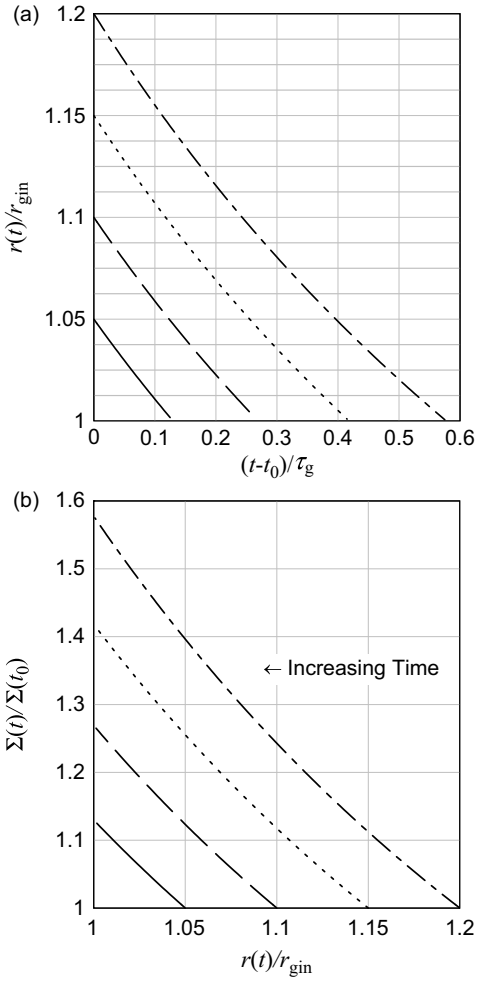

Figure 4. (a) Disc radius as a function of time. As an example, the top line starts at $1.2r_{gin}$ and after a time of around $0.58\tau_g$ this section of the contracting disc reaches the inner gap radius (r_{gin}).(b) The change in surface density as the gap forms. For example, the top line starts at a distance of $1.2r_{gin}$. As the gap forms, the disc radius contracts towards the inner gap radius and the disc surface density increases to near 1.6 times the original disc surface density.

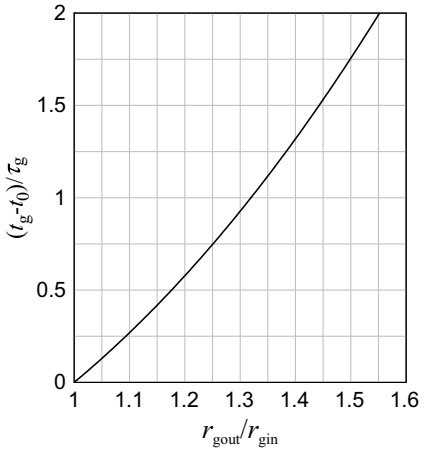

Figure 5. Gap formation time as a function of gap width, where t_G is the total time for the gap to appear, τ_g is the timescale for disc gap formation, while r_{gout} and r_{gin} are, respectively, the outer and inner radii of the gap

https://doi.org/10.1017/pasa.2023.55 Published online by Cambridge University Press

The gap is fully formed at $t = t_G$ and

$$\Sigma_B(r_{gin}, t_G) \approx \frac{2r_{gin}\Sigma(r_{gout}, t_0)}{5\Delta_B}\left(\left(\frac{r_{gout}}{r_{gin}}\right)^{5/2} - 1\right) + \Sigma_B(r_{gin}, t_0). \tag{23}$$

If $\Sigma(r_{gout}, t_0) \approx \Sigma_B(r_{gin}, t_0)$ then

$$\begin{aligned}\frac{\Sigma_B(r_{gin}, t_G)}{\Sigma_B(r_{gin}, t_0)} &\approx \frac{2r_{gin}}{5\Delta_B}\left(\left(\frac{r_{gout}}{r_{gin}}\right)^{5/2} - 1\right) + 1 \\ &= 40\,\frac{1}{(\Delta_B/0.01\,r_{gin})}\left(\left(\frac{r_{gout}}{r_{gin}}\right)^{5/2} - 1\right) + 1.\end{aligned} \tag{24}$$

If $\Delta_B \ll r_{gin}$ then the increase in surface density in the B (boundary) region could be quite significant. In equation (24), we have set $\Delta_B = 0.01\ r_{gin}$ as an example of the possible over-density of material of approximately a factor 40 in the B region of the gap. This over-density could be enhanced in the inner regions of the disc, where the ratio r_{gout}/r_{gin} may be relatively large. Such a density enhancement is also a local pressure maximum and would act as a dust/particle trap thereby increasing the possibility of planetesimal/planet formation.

So, the earliest stages of planet formation may arise on the proximal (i.e., closer to the protostar) edge of a disc gap. However, the distal (i.e., the farthest) edge of the resulting gap will also act as a pressure maximum and dust trap. Either way, infall may produce a gap in the disc where the edges of the resulting gap are prime sites for planet formation.

The formation of gaps by this infall process would essentially be semi-random in terms of radial distance from the protostar. If we ignore the, possibly important, influence of gas drag above the disc, the ballistic path of a particle that is ejected from a disc wind/jet is strongly dependent on the initial vertical (i.e., perpendicular to the midplane) speed of the particle (Liffman & Brown, 1995; Liffman et al., 2020). For a system of particles with a mean size and density, a 'high' jet speed could eject the particles from a protostellar system or to the outer regions of a protostellar disc. A 'low' jet speed would transport particles to the more inner regions of the disc. The resulting radial position of gap would be dependent on random fluctuations in the mean jet/wind speed.

3.1. Enriched concentration of processed dust and pebbles

In the outflow picture of dust infall, dust and pebbles from the inner disc are ejected by an outflow and/or disc wind. This material is observed to be processed by stellar radiation and/or thermal activity in the inner disc. As the disc gap increases in size, the concentration of processed material in the contracting disc between r_{gin} and r_{gout} will increase, as will the concentration of processed material in the B region (Figure 3).

The mass of original material (i.e., dust and gas), M_G in the gap between r_{gin} and r_{gout} is approximately

$$M_G \approx \Sigma_G \pi \left(r_{gout}^2 - r_{gin}^2\right), \tag{25}$$

where Σ_G is the disc surface density in the gap - which, in this case, is assumed to be approximately constant between r_{gin} and r_{gout}. After the gap is formed, the mass of the material at B is given by equation (21). If we assume that the boundary layer B is sufficiently small, we can ignore the initial amount of material in the B region:

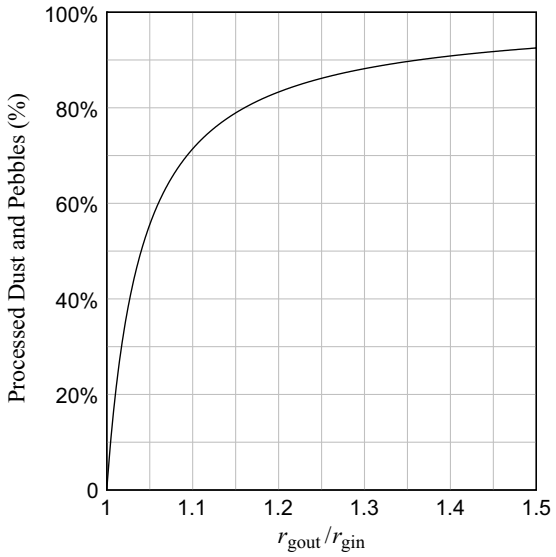

Figure 6. The mass enrichment in the boundary layer B of processed infall dust and pebbles relative to the original dust in the gap, as a function of the ratio of the outer gap distance to the inner gap distance: r_{gout}/r_{gin}. If this gap ratio is, for example, 1.2 then approximately 83% of the material in the B region is composed of processed dust and pebbles.

$M_B(t_0)$, so the mass of processed infall dust and pebbles at B, M_{Bi}, is

$$M_{Bi} \approx M_B(t_G) - M_B(t_0) - M_G \tag{26}$$

The ratio of processed dust and pebbles at B to the original mass of dust in the gap, R_{BiG}. is

$$\begin{aligned}R_{BiG} = \frac{M_{Bi}}{f_{dg}M_G} &\approx \frac{M_B(t_G) - M_B(t_0) - M_G}{f_{dg}M_G} \\ &= \frac{1}{f_{dg}}\left(\frac{4\left(\left(\frac{r_{gout}}{r_{gin}}\right)^{5/2} - 1\right)}{5\left(\left(\frac{r_{gout}}{r_{gin}}\right)^{2} - 1\right)} - 1\right),\end{aligned} \tag{27}$$

where $f_{dg} \approx 0.01$ is the dust to gas mass ratio in the disc.

The enrichment of processed dust and pebbles at B:

$$\frac{M_{Bi}}{f_{dg}M_G + M_{Bi}}. \tag{28}$$

as a function of the gap distance ratio: r_{gout}/r_{gin} is shown in Figure 6. Here we can see that a gap distance ratio of 1.1 would imply that approximately 70% of the material in the B region was composed of processed dust and pebbles. Such a result may have application in the early solar system: if plantesimals formed from 'B' region material, then most of the material we observe in primitive meteorites and comets may have been preprocessed dust and pebbles.

3.2. Dust traps

A difficulty in the scenario that is schematically depicted in Figure 3 is that the concentrated dust in the boundary 'B' region may simply move out of the region due to radial drif t on timescales that are shorter then the formation timescale of the 'B'

https://doi.org/10.1017/pasa.2023.55 Published online by Cambridge University Press

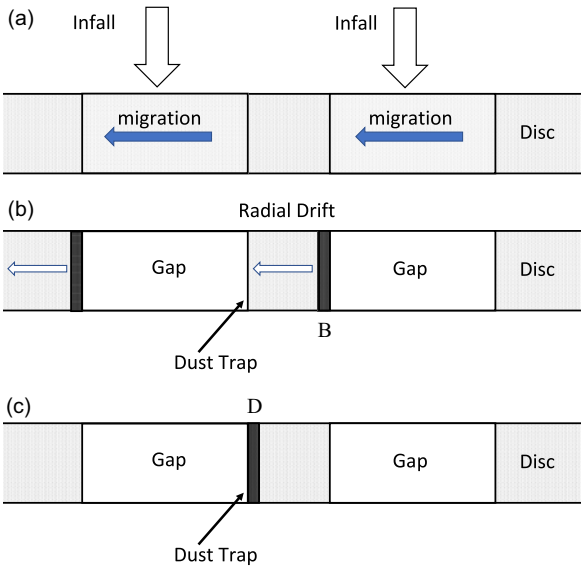

Figure 7. (a) Infalling material rains down on two separate sections of a disc, thereby inducing radial migration of material into boundary layers located at the inner gap edges. (b) If the infall proceeds for a sufficiently long period of time, gaps, or low-density regions may form with a high-density region or pressure maximum region B at the inner edge of the gaps. During the formation of these high-density regions, the particulate material may radially drift towards the protostar. (c) Particulate material is subsequently trapped in the D (dust trap) region which naturally forms at the outer edge of the inner gap. Both the B and D regions may have an over abundance of particulate material that is advantageous for planetesimal formation.

region. This would not be an opportune situation for planet formation. As noted previously, the outer edge of the gap in Figure 3 will naturally act as a dust drap, due to the increase in pressure gradient between the gap and the disc.

So, another possibility is that the infall of material forms two gaps instead of one as is illustrated in Figure 7. In this case, the particulate material from the outer gap can potentially be trapped by the outer edge of the inner gap. To obtain an indication of the drift time required for a particle of a certain size and density, we consider a ring of material that is created between two gaps.

From Appendix D, the drift time for particles in a model disc is

$$t - t_0 \approx \tau_{\rm drift}\left(\left(\frac{r_0}{r}\right)^{3/4} - \left(\frac{r_0}{r_{t_0}}\right)^{3/4}\right), \qquad (29)$$

with t_0 the initial time, r_{t_0} the initial position of the particle, and $r_0 = 1$ au is the distance scale used in our model disc (Appendix D).

The drift timescale $\tau_{\rm drift}$ is given by:

$$\tau_{\rm drift} = \frac{8 r_0^2 \mu m_{\rm H}}{21 \tau_{s0} k_{\rm BP} T_{g0}} \approx 1.5 \times 10^5 \left(\frac{1\ {\rm mm}}{a_{\rm p}}\right) {\rm yrs}, \qquad (30)$$

here, $k_{\rm BP}$ the Boltzmann constant, μ the mean molecular mass (≈ 2.3), $m_{\rm H}$ the hydrogen atom mass, τ_{s0} is the scale factor for the stopping time and T_{g0} is a scale factor (= 500 K) for the temperature of the gas (see Appendix D).

Equation (29) is approximately valid for a particle with a radius less than about a metre. Equation (30) indicates that particles with radii less than about 1 mm are going to have drift times that tend to be comparable to or in excess of the gap formation time scales. This also depends, of course, on the width of the disc ring between the two gaps. Noting that caveat, particles with radii less than 0.1 mm will tend to stay in the compressed B regions, while larger particles will have a greater chance of being caught in a inter-gap dust trap D (Figure 7).

4. Discussion

There is a growing body of evidence that refractory, particulate material like Forsterite (Mg_2SiO_4) dust is ejected from the inner disc regions of protostellar systems (possibly between 0.3 and 0.7 au for the protostellar system EX Lup) and is either completely ejected from the protostellar system (e.g., HOPS-68 (Poteet et al., 2011)) or lands back in the disc around 3 au (for EX Lup) from the ejection point near the star (Juhász et al., 2012; Ábrahám et al., 2019; Kóspál et al., 2023).

The physical mechanisms that eject particulate material from accretion discs have been debated over many years. These mechanisms include stellar winds (Herbig, 1977), disc winds (Liffman, 1992; Liffman & Brown, 1995, 1996; Shu et al., 1996; Hu, 2010; Bans & Königl, 2012; Salmeron & Ireland, 2012; Miyake et al., 2016; Giacalone et al., 2019), photophoresis (Krauss & Wurm, 2005; Cuello et al., 2016), photoevaporation (Hutchison et al., 2016) and radiation pressure combined with disc winds (Vinković & Čemeljić, 2021). The complexity of the physics is such that *all* of these processes may play a role depending on the material that is being ejected and where in the disc the material is located. Regardless of the physical mechanisms that drive this ejection process, once the particles start moving freely across the face of the accretion disc, their orbital angular momentum should become small relative to their radial position in the accretion disc.

We have found that the infall of ejected, processed low angular momentum dust/pebbles/gas from a protostellar jet and/or disc wind onto a discrete, somewhat random region of a protostellar disc can produce a disc gap on a timescales of of 10^5 to 10^6 years (Section 3). This may, partially, answer the question of how the observed gaps and rings can form in even the youngest protostellar systems (van der Marel et al., 2019). Infall of low angular momentum material from a nascent molecular cloud onto a protostellar system may also produce the same effect (Kuznetsova et al., 2022).

The infall of low angular momentum material onto a protostellar disc can produce disc gaps, which then lead to over-dense regions on the inner or outer edges of the gaps, which encourage planet formation. Infall is the 'chicken' that lays the 'egg' of planet formation.

The original disc material in the gap plus the infalling material, can be compressed onto the inner edge of the gap, that is, the 'B' boundary region of Figure 3, where most of the solid material in this compressed B region consists of processed dust and pebbles (Figure 6). Another possibility is that mulitple gaps form, due to the non-uniform infall of material over a disc interval and that material drifts through a thin disc ring, to be trapped in the 'D' dust trap region on the other side of the ring (Figure 7).

In the more parochial context of the formation Solar System, this B region could contain O^{16}-rich material (e.g., Calcium Aluminium Inclusions (CAIs) and Amoeboid Olivine Aggregates (AOAs)) which likely formed near the protoSun/inner edge of the disc (Liffman et al., 2016; Larsen et al., 2020) plus processed, O^{16}-poor, forsterite dust from the inner disc regions. In this case, the CAIs/AOAs could be ejected from the interaction between the solar magnetosphere and the inner edge/region of the solar accre-

https://doi.org/10.1017/pasa.2023.55 Published online by Cambridge University Press

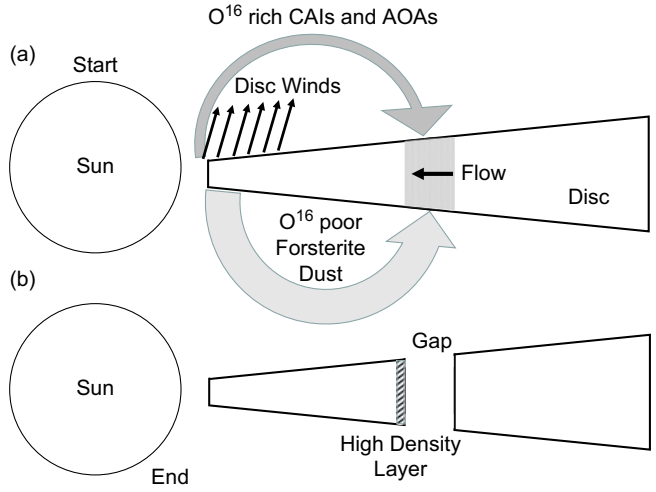

Figure 8. (a) The disc gaps would be produced from processed infall material. In the context of the early Solar System, the jet flows closest to the protoSun, ejected Calcium Aluminium Inclusions (CAIs) and Amoeboid Olivine Aggregates (AOAs) that are both enriched with O^{16}, where the ratio of oxygen isotopes are similar to those found in the Sun (McKeegan et al., 2011). Observations from EX Lup suggest that disc winds between 0.3 and 0.7 au from the star, eject/process amorphous silicate into crystalline forsterite that lands further away from the protoStar. In the Solar System, such forsterite would very probably be O^{16} poor. (b) The subsequent gap formation would concentrate these materials to, potentially, form the base material for pre-chondritic planetesimals

tion disc, while the forsterite grains could be ejected via disc winds produced further from the protoSun.

The resulting gap formation and concentrating of infalling, processed materials would then provide the foundation for pre-chondritic planetesimals. Chondrules and the base materials for chondritic planetesimals might then be produced by collisions between the pre-chondritic planetesimals (Figure 8). This general scenario is qualitatively consistent with the hypothetical formation process required to explain the isotopic diversity observed in carbonaceous chondrites (Hellmann et al., 2023).

5. Conclusions

In this study, we have examined the general case of what happens when low angular momentum material falls onto a protostellar disc. We have used the resulting mass and angular momentum equations (equations (1) and (3)) to derive, for an inviscid disc, a number of quantities including the radial speed of disc material (equation (5)), the rate of mass flow in the disc (equation (6)) and the time evolution of the disc surface density (equation (9)).

We then assume that the source of this infalling low angular momentum material onto the protoplanetary disc is the ejection of, mainly, particulate material from the inner disc regions, where this ejected, relatively low angular momentum, material subsequently falls onto the outer disc regions. Such particle ejection and transport is consistent with observations and long standing theoretical predictions. Equations (5) and (9) are then applied to the formation of disc rings and gaps (Section 3). Using the derived equations, we show that the recycling of infalling material is probably not large enough to drive the observed accretion flow from a protostellar disc onto its protostar. However, infall can produce gaps/rings in discs on timescales of 10^5 to 10^6 years.

The formation of gaps and rings occurs when infalling, low angular momentum material lands on a discrete section of the disc instead of the entire disc surface. Such a phenomenon is consistent with observations. The affected section of the disc then moves towards the protostar and the disc material will slowly ram into the adjacent, interior disc, which is not suffering the influence of infalling material. This process may produce an over abundance of material in a compressed layer on the inner edge of the gap (Section 3.1). The amount of enrichment can be significant. For example, if the ratio of the radius of the outer edge to the inner edge of the gap is 1.1 then about 70% of the solid material in the compressed layer is composed of processed dust and pebbles from the inner regions of the disc (Figure 6).

Alternatively, infall may be somewhat random in space and time thereby producing multiple gaps. In such a circumstance, particulate material may drift from the inner edge of an outer gap, to the outer edge of an adjacent, inner gap (Figure 7). The outer edge of a gap is a natural dust trap. Reasonable drift timescales tend to be applicable for particles greater than 0.1 mm in radius, where our analysis has only considered particles less than a metre in radius (Section 3.2).

We suggest that gap formation due to infall lays the foundation for planetesimal formation by compressing the material in the gap to the inner edge of the gap or, via radial drift, to the adjacent outer edge of another gap. Gaps can be produced on relatively short timescales from the inception of the protostellar system.

In our protosolar system, such a process may have collected O^{16}-poor forsterite dust from the inner regions of the protosolar disc and O^{16}-rich CAIs and AOAs from the inner edge regions of the protosolar disc, thereby constructing a region favourable to the formation of pre-chondritic planetesimals.

Acknowledgement. I thank Professor Sarah Maddison, Dr Geoffrey Bryan and our talented colleagues at Swinburne University's Centre for Astronomy and Supercomputing for their friendship, collaboration, and support. I also thank the anonymous reviewer for his/her constructive comments that greatly improved the manuscript.

References

Ábrahám, P., Chen, L., Kóspál, Á., et al. 2019, ApJ, 887, 156
Bai, X.-N. 2016, ApJ, 821, 80
Balbus, S. A., & Hawley, J. F. 1991, ApJ, 376, 214
Bans, A., & Königl, A. 2012, ApJ, 758, 100
Bizzarro, M., Connelly, J. N., & Krot, A. N. 2017, in Astrophysics and Space Science Library, Vol. 445, Formation, Evolution, and Dynamics of Young Solar Systems, ed. M. Pessah & O. Gressel, 161
Borlina, C. S., Weiss, B. P., Bryson, J. F. J., et al. 2021, Science Advances, 7, eabj6928
Brauer, F., Dullemond, C. P., & Henning, T. 2008, A&A, 480, 859
Brauer, F., Dullemond, C. P., Johansen, A., et al. 2007, A&A, 469, 1169
Cuello, N., Gonzalez, J. F., & Pignatale, F. C. 2016, MNRAS, 458, 2140
Falcke, H., & Melia, F. 1997, ApJ, 479, 740
Flaherty, K. M., Hughes, A. M., Rose, S. C., et al. 2017, ApJ, 843, 150
Frank, J., King, A., & Raine, D. J. 2002, Accretion Power in Astrophysics: Third Edition (Cambridge University Press)
Fromang, S., & Lesur, G. 2019, in EAS Publications Series, Vol. 82, EAS Publications Series, 391–413
Giacalone, S., Teitler, S., Königl, A., Krijt, S., & Ciesla, F. J. 2019, ApJ, 882, 33
Hansen, B. M. S. 2014, MNRAS, 440, 3545
Hayashi, C. 1981, Progr. Theor. Phys. Suppl., 70, 35
Hellmann, J. L., Schneider, J. M., Wölfer, E., et al. 2023, ApJ, 946, L34
Herbig, G. H. 1977, ApJ, 217, 693
Hu, R. 2010, ApJ, 725, 1421
Hutchison, M. A., Price, D. J., Laibe, G., & Maddison, S. T. 2016, MNRAS, 461, 742

https://doi.org/10.1017/pasa.2023.55 Published online by Cambridge University Press

Juhász, A., Dullemond, C. P., van Boekel, R., et al. 2012, ApJ, 744, 118
Kóspál, Á., Ábrahám, P., Diehl, L., et al. 2023, ApJ, 945, L7
Krauss, O., & Wurm, G. 2005, ApJ, 630, 1088
Kuznetsova, A., Bae, J., Hartmann, L., & Mac Low, M.-M. 2022, ApJ, 928, 92
Larsen, K. K., Wielandt, D., Schiller, M., Krot, A. N., & Bizzarro, M. 2020, Earth and Planetary Science Letters, 535, 116088
Li, J., & Wickramasinghe, D. T. 1997, in Astronomical Society of the Pacific Conference Series, Vol. 121, IAU Colloq. 163: Accretion Phenomena and Related Outflows, ed. D. T. Wickramasinghe, G. V. Bicknell, & L. Ferrario, 241
Liffman, K. 1992, Icarus, 100, 608
Liffman, K., & Brown, M. 1995, Icarus, 116, 275
Liffman, K., & Brown, M. J. I. 1996, in Chondrules and the Protoplanetary Disk, 285–302
Liffman, K., Bryan, G., Hutchison, M., & Maddison, S. T. 2020, MNRAS, 493, 4022
Liffman, K., Cuello, N., & Paterson, D. A. 2016, MNRAS, 462, 1137
Liffman, K., & Toscano, M. 2000, Icarus, 143, 106
Macías, E., Guerra-Alvarado, O., Carrasco-González, C., et al. 2021, A&A, 648, A33
Martin, R. G., Nixon, C. J., Pringle, J. E., & Livio, M. 2019, New A, 70, 7
McKeegan, K. D., Kallio, A. P. A., Heber, V. S., et al. 2011, Science, 332, 1528
Miyake, T., Suzuki, T. K., & Inutsuka, S.-I. 2016, ApJ, 821, 3
Nakagawa, Y., Sekiya, M., & Hayashi, C. 1986, Icarus, 67, 375
Ohashi, S., & Kataoka, A. 2019, ApJ, 886, 103
Pinilla, P., Birnstiel, T., Ricci, L., et al. 2012, A&A, 538, A114
Poteet, C. A., Megeath, S. T., Watson, D. M., et al. 2011, ApJ, 733, L32
Salmeron, R., & Ireland, T. 2012, M&PS, 47, 1922
Segura-Cox, D. M., Schmiedeke, A., Pineda, J. E., et al. 2020, Nature, 586, 228
Shakura, N. I., & Sunyaev, R. A. 1973, A&A, 24, 337
Shu, F. H., Shang, H., & Lee, T. 1996, Science, 271, 1545
Teague, R., Henning, T., Guilloteau, S., et al. 2018, ApJ, 864, 133
van der Marel, N., Dong, R., di Francesco, J., Williams, J. P., & Tobin, J. 2019, ApJ, 872, 112
Vinković, D., & Čemeljić, M. 2021, MNRAS, 500, 506
Weidenschilling, S. J. 1977, MNRAS, 180, 57
Weiss, B. P., Bai, X.-N., & Fu, R. R. 2021, Sci. Adv., 7, eaba5967
Wijnen, T. P. G., Pols, O. R., Pelupessy, F. I., & Portegies Zwart, S. 2017, A&A, 602, A52
Williams, J. P., & Cieza, L. A. 2011, ARA&A, 49, 67
Zhou, T., Deng, H.-P., Chen, Y.-X., & Lin, D. N. C. 2022, ApJ, 940, 117

Appendix A. Mass and angular conservation equations

A.1. Mass conservation

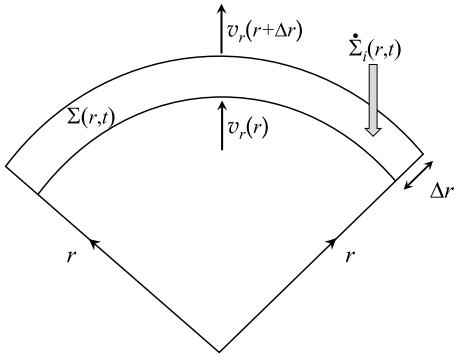

Figure 9. Schematic of a disc differential ring that illustrates the disc mass conservation equation with infall.

From Figure 9,

$$\begin{aligned} 2\pi r\Delta r\frac{\partial \Sigma}{\partial t} &= 2\pi r v_{\rm r}(r,t)\Sigma(r,t) \\ &\quad - 2\pi (r+\Delta r)v_{\rm r}(r+\Delta r,t)\Sigma(r+\Delta r,t) \\ &\quad + 2\pi r\Delta r\dot{\Sigma}_{\rm i}(r,t) \end{aligned} \tag{31}$$

dividing both sides by $2\pi r\Delta r$ and allowing $\Delta r \to 0$ gives the disc mass conservation:

$$\frac{\partial \Sigma}{\partial t} = -\frac{1}{r}\frac{\partial\,(rv_{\rm r}\Sigma)}{\partial r} + \dot{\Sigma}_{\rm i}. \tag{32}$$

A.2. Angular momentum conservation

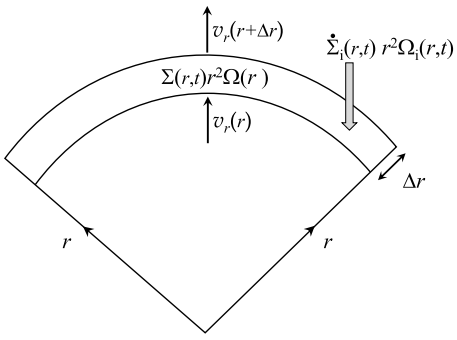

Figure 10. Schematic of a disc differential ring that illustrates the disc angular momentum conservation equation with infall.

From Figure 10,

$$\begin{aligned} &2\pi r\Delta r\frac{\partial\left(\Sigma r^2\Omega\right)}{\partial t} = 2\pi r v_{\rm r}(r,t)\Sigma(r,t)r^2\Omega \\ &- 2\pi (r+\Delta r)v_{\rm r}(r+\Delta r,t)\Sigma(r+\Delta r,t)(r+\Delta r)^2\Omega(r+\Delta r) \\ &+ \Delta r\frac{\partial Q}{\partial r} + 2\pi r\Delta r\dot{\Sigma}_{\rm i}(r,t)r^2\Omega_{\rm i}(r,t), \end{aligned} \tag{33}$$

which gives the angular momentum conservation equation:

$$\begin{aligned} \frac{\partial\left(\Sigma r^2\Omega\right)}{\partial t} &= -\frac{1}{r}\frac{\partial\left(rv_{\rm r}\Sigma r^2\Omega\right)}{\partial r} \\ &\quad + \frac{1}{2\pi r}\frac{\partial Q}{\partial r} + \dot{\Sigma}_{\rm i}r^2\Omega_{\rm i}. \end{aligned} \tag{34}$$

Appendix B. Disc accretion speed

From equation (32),

$$\frac{\partial(v_{\rm r}\Sigma r^3\Omega)}{\partial r} = r^2\Omega\left(r\dot{\Sigma}_{\rm i} - r\frac{\partial\Sigma}{\partial t}\right) + rv_{\rm r}\Sigma\frac{\partial(r^2\Omega)}{\partial r}, \tag{35}$$

while

$$\frac{\partial\left(\Sigma r^2\Omega\right)}{\partial t} = \frac{\partial\Sigma}{\partial t}r^2\Omega. \tag{36}$$

Combining these equations with equation (34)

$$\begin{aligned} r\frac{\partial\left(\Sigma r^2\Omega\right)}{\partial t} &+ \frac{\partial\left(rv_{\rm r}\Sigma r^2\Omega\right)}{\partial r} \\ &= \dot{\Sigma}_{\rm i}r^3\Omega + rv_{\rm r}\Sigma\frac{\partial\left(r^2\Omega\right)}{\partial r} \\ &= \frac{1}{2\pi}\frac{\partial Q}{\partial r} + \dot{\Sigma}_{\rm i}r^3\Omega_{\rm i}, \end{aligned} \tag{37}$$

https://doi.org/10.1017/pasa.2023.55 Published online by Cambridge University Press

and so,

$$r v_r \Sigma \frac{\partial \left(r^2\Omega\right)}{\partial r} = \frac{1}{2\pi}\frac{\partial Q}{\partial r} + \dot{\Sigma}_i r^3 \left(\Omega_i - \Omega\right), \tag{38}$$

or

$$v_r = \frac{1}{r\Sigma \frac{\partial\left(r^2\Omega\right)}{\partial r}}\left(\frac{1}{2\pi}\frac{\partial Q}{\partial r} + \dot{\Sigma}_i r^3 \left(\Omega_i - \Omega\right)\right). \tag{39}$$

We apply our inviscid disc assumption: $Q \approx 0$ and obtain

$$\begin{aligned} v_r &= \frac{1}{r\Sigma \frac{\partial\left(r^2\Omega\right)}{\partial r}}\left(\dot{\Sigma}_i r^3 \left(\Omega_i - \Omega\right)\right) \\ &= \frac{1}{\frac{\partial\left(r^2\Omega\right)}{\partial r}}\frac{\dot{\Sigma}_i}{\Sigma} r^2 \left(\Omega_i - \Omega\right). \end{aligned} \tag{40}$$

Appendix C. Analytic solutions of the disc equations for the case $\Omega_i \approx 0$ and constant $\dot{\Sigma}_i$

In this case, (5) becomes

$$v_r = \frac{dr}{dt} = -2r\frac{\dot{\Sigma}_i}{\Sigma}, \tag{41}$$

while equation (9) has the form

$$\frac{\partial \Sigma}{\partial t} = 5\dot{\Sigma}_i. \tag{42}$$

We can eliminate $\dot{\Sigma}_i$ from both equations and obtain

$$\frac{1}{\Sigma}\frac{\partial \Sigma}{\partial t} = \frac{-5}{2r}\frac{dr}{dt}, \tag{43}$$

which has the solution

$$\Sigma(r(t), t) = \Sigma(r(t_0), t_0)\left(\frac{r(t_0)}{r(t)}\right)^{\frac{5}{2}}, \tag{44}$$

Substituting equation (44) into equation (41) and using the assumption that $\dot{\Sigma}_i$ is a constant gives

$$r(t) = \frac{r(t_0)}{\left(1 + 5\frac{\dot{\Sigma}_i}{\Sigma(r(t_0),t_0)}(t - t_0)\right)^{2/5}}. \tag{45}$$

Substituting equation (45) into equation (44) implies

$$\Sigma(r(t), t) = \Sigma(r(t_0), t_0) + 5\dot{\Sigma}_i(t - t_0). \tag{46}$$

Appendix D. Drift equations

From Nakagawa et al. (1986), the radial drift speed for particles, v_{dr}, is given by

$$v_{dr} = \frac{\rho_g \tau_s \frac{dp}{dr}}{\left(\rho_g + \rho_d\right)^2 + \rho_g^2 \tau_s^2 \Omega^2}, \tag{47}$$

with ρ_g the spatial gas mass density, ρ_d the spatial particle mass density, $\frac{dp}{dr}$ the gas radial pressure gradient, τ_s the particle stopping time and Ω the Keplerian angular frequency.

Assuming Epstein drag, the stopping time is

$$\tau_s \approx \frac{a_p \rho_p}{(1 + \pi/8)\ \rho_g v_{th}}, \tag{48}$$

here, a_p is the particle radius, ρ_p is the particle density (set to 3 000 kgm^{-3}), the $1 + \pi/8$ is a correction factor for the Epstein drag coefficient (Liffman & Toscano, 2000), and v_{th} is the thermal gas speed, where

$$v_{th} = \sqrt{\frac{8 k_{BP} T_g}{\pi \mu m_H}}, \tag{49}$$

with k_{BP} the Boltzmann constant (where the P notes Planck as the person who actually proposed the constant), μ the mean molecular mass (≈ 2.3), m_H the hydrogen atom mass and T_g the temperature of the gas.

For our disc model, we assume that

$$\rho_g(r) = \rho_{g0}\left(\frac{r_0}{r}\right)^{\alpha}, \tag{50}$$

with $r_0 = 1$ au, ρ_{g0} is set to 10^{-6} kg m^{-3} and $\alpha = 3$.

$$T_g(r) = T_{g0}\left(\frac{r_0}{r}\right)^{\beta}, \tag{51}$$

with $T_{g0} = 500$ K and $\beta = 1/2$

The values of $\rho_{g0}, T_{g0}, \alpha$ and β are chosen to produce a disc surface density that is approximately similar to the Hayashi minimum mass surface density for the solar system protoplanetary disc (Hayashi, 1981):

$$\Sigma_{Hayashi}(r) = 1\,700\left(\frac{r_0}{r}\right)^{3/2}\ \text{g cm}^{-3}. \tag{52}$$

In our case, we used the model surface density:

$$\Sigma_{model}(r) \approx 2\rho_g(r)h(r), \tag{53}$$

where $h(r)$ is the scale height of the disc:

$$h(r) \approx \sqrt{\frac{2r^3 k_{BP} T_g(r)}{\mu m_H G M_*}}. \tag{54}$$

To determine the pressure gradient in equation (47), we note that the gas pressure is

$$p(r) = \frac{k_{BP}\rho_g(r)T_g(r)}{\mu m_H}. \tag{55}$$

Substituting equations (50) and (51) gives

$$\frac{dp}{dr} = -(\alpha + \beta)\frac{k_{BP}\rho_g(r)T_g(r)}{\mu m_H r}. \tag{56}$$

Substituting this equation into equation (47), and ignoring the ρ_d/ρ_g term as it is ~ 0.01, gives

$$v_{dr} \approx \frac{-(\alpha + \beta)\ \tau_s k_{BP} T_g(r)}{\mu m_H r\left(1 + \tau_s^2\Omega^2\right)}, \tag{57}$$

From equations (49) and (51)

$$v_{th} = \sqrt{\frac{8 k_{BP} T_{g0}}{\pi \mu m_H}}\left(\frac{r_0}{r}\right)^{\beta/2} \equiv v_{th0}\left(\frac{r_0}{r}\right)^{\beta/2}. \tag{58}$$

Similarly,

$$\tau_s \approx \frac{a_p \rho_p}{(1 + \pi/8)\ \rho_{g0} v_{th0}}\left(\frac{r_0}{r}\right)^{-\alpha-\beta/2} \equiv \tau_{s0}\left(\frac{r_0}{r}\right)^{-\alpha-\beta/2}. \tag{59}$$

Combining equations (51), (59), and (57) plus defining $\Omega_0^2 = GM_*/r_0^3$, gives

$$v_{dr} \approx \frac{-(\alpha + \beta)\ \tau_{s0} k_{BP} T_{g0}\left(\frac{r_0}{r}\right)^{-\alpha+\beta/2+1}}{\mu m_H r_0\left(1 + \tau_{s0}^2\Omega_0^2\left(\frac{r_0}{r}\right)^{-2\alpha-\beta+3}\right)}. \tag{60}$$

https://doi.org/10.1017/pasa.2023.55 Published online by Cambridge University Press

Defining

$$A = \frac{(\alpha+\beta)\,\tau_{s0} k_{BP} T_{g0}}{\mu m_H r_0}, \tag{61}$$

and

$$B = \tau_{s0}^2 \Omega_0^2, \tag{62}$$

implies

$$v_{dr} = \frac{dr}{dt} \approx \frac{-A\left(\frac{r_0}{r}\right)^{-\alpha+\beta/2+1}}{\left(1+B\left(\frac{r_0}{r}\right)^{-2\alpha-\beta+3}\right)}. \tag{63}$$

$$\Longrightarrow$$

$$\left(\left(\frac{r_0}{r}\right)^{\alpha-\beta/2-1} + B\left(\frac{r_0}{r}\right)^{-\alpha-3\beta/2+2}\right)\frac{dr}{dt} \approx -A. \tag{64}$$

$$\Longrightarrow$$

$$\begin{aligned}&\left(\frac{1}{r_0}\right)^{-\alpha+\beta/2+1}\frac{\left(r^{-\alpha+\beta/2+2} - r_{t0}^{-\alpha+\beta/2+2}\right)}{-\alpha+\beta/2+2}\\ &+ B\left(\frac{1}{r_0}\right)^{\alpha+3\beta/2-2}\frac{\left(r^{\alpha+3\beta/2-1} - r_{t0}^{\alpha+3\beta/2-1}\right)}{\alpha+3\beta/2-1}\\ &\approx -A(t-t_0),\end{aligned} \tag{65}$$

where t_0 is the initial time and r_{t0} is the initial position of the particle.

For $\alpha = 3$ and $\beta = 1/2$

$$\begin{aligned}&\left(\frac{r_0}{r}\right)^{3/4} - \left(\frac{r_0}{r_{t0}}\right)^{3/4} - \frac{3B}{11}\left(\left(\frac{r}{r_0}\right)^{11/4} - \left(\frac{r_{t0}}{r_0}\right)^{11/4}\right)\\ &\approx \frac{3A}{4r_0}(t-t_0).\end{aligned} \tag{66}$$

For particle radii less than approximately 1 m, $B \ll 1$, so

$$\left(\frac{r_0}{r}\right)^{3/4} - \left(\frac{r_0}{r_{t0}}\right)^{3/4} \approx \frac{3A}{4r_0}(t-t_0), \tag{67}$$

and

$$t - t_0 \approx \tau_{drift}\left(\left(\frac{r_0}{r}\right)^{3/4} - \left(\frac{r_0}{r_{t0}}\right)^{3/4}\right), \tag{68}$$

with

$$\begin{aligned}\tau_{drift} &= \frac{4r_0}{3A} = \frac{8r_0^2 \mu m_H}{21\tau_{s0} k_{BP} T_{g0}}\\ &\approx 1.5\times 10^5 \left(\frac{1\text{ mm}}{a_p}\right)\text{ yrs.}\end{aligned} \tag{69}$$

https://doi.org/10.1017/pasa.2023.55 Published online by Cambridge University Press